

Impact of Full Duplex Scheduling on End-to-End Throughput in Multi-Hop Wireless Networks

Xiaoqi Qin, *Student Member, IEEE*, Huacheng Zeng, *Member, IEEE*, Xu Yuan, *Member, IEEE*, Brian Jalaian, *Member, IEEE*, Y. Thomas Hou, *Fellow, IEEE*, Wenjing Lou, *Fellow, IEEE*, and Scott F. Midkiff, *Senior Member, IEEE*

Abstract—There have been some rapid advances on the design of full duplex (FD) transceivers in recent years. Although the benefits of FD have been studied for single-hop wireless communications, its potential on throughput performance in a multi-hop wireless network remains unclear. As for multi-hop networks, a fundamental problem is to compute the achievable end-to-end throughput for one or multiple communication sessions. The goal of this paper is to offer some fundamental understanding on end-to-end throughput performance limits of FD in a multi-hop wireless network. We show that through a rigorous mathematical formulation, we can cast the multi-hop throughput performance problem into a formal optimization problem. Through numerical results, we show that in many cases, the end-to-end session throughput in a FD network can exceed $2\times$ of that in a half duplex (HD) network. Our finding can be explained by the much larger design space for scheduling that is offered by removing HD constraints in throughput maximization problem. The results in this paper offer some new understandings on the potential benefits of FD for end-to-end session throughput in a multi-hop wireless network.

Index Terms—Full duplex, wireless multi-hop network, throughput maximization

1 INTRODUCTION

HALF duplex (HD) has been the fundamental limitation in transceiver design since the beginning of wireless communications. Under HD, a transceiver can only tend to one task at a time: transmit or receive. Conceptually, HD cuts down potential throughput by half at a node. Recent breakthrough in full duplex (FD) transceiver design opens up new possibility in wireless communications. The main challenge in the design of a FD transceiver is how to cancel self-interference caused by simultaneous transmission and reception. Recent results have shown various transceiver designs [1], [2], [3], [4] that use a combination of antenna techniques, analog cancellation methods, and digital cancellation methods to suppress the self-interference.

As designs for FD transceivers continue to improve, there is a growing interest in the benefit of FD beyond physical layer, such as FD MAC protocol design [5], [6], [7], [8], [9], [10], [11], [12], [13] and cross-layer optimization problems [14], [15], [16], [17], [18], [19], [20], [21], [22]. The work in [22] presents a recent study on upper layer performance of FD in a multi-hop wireless network. Specifically, in the first part of [22], the authors showed an asymptotic analysis of network capacity under the protocol model. The network capacity is defined as the maximum data rate that can be supported between every source-destination pair (per-flow capacity). The authors concluded that FD cannot double network capacity when the number of nodes goes to infinity. In the second part, the authors investigated the

MAC-layer capacity for finite-sized network with one-hop bidirectional transmissions. The MAC-layer capacity is defined as the total capacity of all bi-directional links in the network. The results showed that with a CSMA-based MAC protocol, the capacity gain of FD over HD is below 2.

Different from [22], the goal of this paper is to offer some fundamental understandings on the end-to-end throughput performance of FD in a finite-sized multi-hop network. In multi-hop networks, a fundamental problem is to compute the achievable end-to-end throughput for one or multiple active sessions. In this paper, we study the impact of FD on end-to-end session throughput in multi-hop networks under *optimal* scheduling through rigorous mathematical formulation. Our results show that the achievable end-to-end session throughput in a FD network can be more than $2\times$ of that in a HD network within their schedulable region (i.e., traffic in both HD and FD networks can be scheduled with nonzero throughput). That is, from end-to-end throughput perspective, $2\times$ is not a fundamental performance barrier of FD in a multi-hop wireless network. This finding is enlightening and not entirely surprising, and can be explained by the much larger design space for optimal scheduling that is offered by removing the HD constraints in the problem formulation.

Our insights on why $2\times$ is not a fundamental limit of FD in multi-hop wireless networks can be explained as follows. For end-to-end session throughput in a multi-hop wireless network, the advantage of FD is not limited to achieving simultaneous transmission and reception at each node. Instead, FD also gives a much larger design space for scheduling compared to HD. Since a session's end-to-end throughput is determined by the capacity of the bottleneck link along its path, therefore, the larger scheduling space offered by FD can help to decrease the mutual interference for the bottleneck link (with fewer interfering links) and

• The authors are with the Virginia Polytechnic Institute and State University, Blacksburg VA 24061.

E-mail: {xiaoqi, zeng, xuy10, bran, thou, wjlou, midkiff}@vt.edu.

Manuscript received 16 July 2015; revised 18 Feb. 2016; accepted 22 Feb. 2016. Date of publication 3 Mar. 2016; date of current version 1 Dec. 2016.

For information on obtaining reprints of this article, please send e-mail to: reprints@ieee.org, and reference the Digital Object Identifier below.

Digital Object Identifier no. 10.1109/TMC.2016.2538232

thus increase its capacity. Note that a node with FD capability does not have to exclude HD scheduling in the optimal solution, if it chooses to. As we shall show in our numerical investigation, the end-to-end throughput ratio under FD over that under HD is no longer bounded by the $2\times$ factor that is associated with a FD node in isolation.

The remainder of this paper is organized as follows. In Section 2, we review related work on FD in physical layer design, MAC layer protocol design, and network layer performance analysis, respectively. In Section 3, we present a mathematical model for a FD multi-hop network. Based on this model, we present a problem formulation for a throughput maximization problem. In Section 4, we reformulate the problem to a simpler mathematical form, which can be solved by a commercial solver such as CPLEX. In Section 5, we conduct numerical investigation on end-to-end throughput performance of FD in a multi-hop wireless network. Section 6 concludes this paper.

2 RELATED WORK

To demonstrate the feasibility of FD, various transceiver designs have been proposed. Note that simultaneous transmission and reception requires a wireless transceiver to have both the transmit and receive radio-frequency (RF) chains. There are two ways to separate these two RF chains [23]. One method is physically separating the transmit and receive antenna from one another in a separate-antenna system [2], [6], [24]. The other method is to use a circulator in a shared-antenna system [25]. However, the level of isolation provided by the above methods is not enough to extract the signal of interest from the self interference caused by signal leaking from its transmit RF chain to its receive RF chain. Therefore, the key challenge in enabling a transceiver to operate in FD mode is how to cancel self interference. Practical self-interference cancellation schemes usually use a combination of passive and active methods. Passive methods aim to suppress the self-interference before it enters the receive RF chain circuit by using various antenna techniques [2], [24], [25], [26], [27], [28], [29]. Active methods employ the knowledge of transmit signals and subtract it from the received signal, and can be classified into analog cancellation and digital cancellation. Analog cancellation aims to subtract the estimated self-interference signal in the analog receive circuit before the ADC [1], [3], [4], [24], [30], [31], [32]. Digital cancellation aims to subtract the estimate self-interference signal after ADC in the digital domain [31], [33], [34], [35]. The current state-of-art FD transceiver design is the one in [1] by Bharadia et al. This design only requires a single antenna and is closest to what one would wish to have from a FD node. It can achieve 110 dB of self-interference cancellation and thus meets the requirements of 802.11 standards.

To translate the benefit of FD in physical layer to upper layers, various MAC layer protocol designs have been proposed for both infrastructure networks and ad hoc networks. As for infrastructure networks, centralized MAC protocols are designed to manage the inter-user interference caused by simultaneous transmission and reception of access point (AP) and the hidden terminal problem caused by asymmetric data traffic [4], [5], [6], [7]. As for ad hoc networks, distributed MAC protocols

are designed to support bi-directional links and two-hop relay transmissions [9], [8], [10], [11] as wells as multi-hop communications [12], [13].

Throughput performance analysis for various types of FD networks have been studied. In [14], Tong and Haenggi investigated the throughput performance for a FD wireless network consists of single-hop links. The authors quantified the impact of imperfect self-interference cancellation on the throughput gain of FD networks over HD networks under ALOHA protocol. In [15], Lee and Quek characterized the throughput of hybrid-duplex heterogeneous networks composed of multi-tier networks with APs operating in either FD bi-directional mode or HD downlink mode. The authors investigated the effect of AP spatial density and transmission power on the network throughput. In [16], Wang et al. established a spatial stochastic framework to investigate the network throughput gain of FD in multi-cell networks with contending single-hop links. The authors characterized the FD gain in terms of link distance, interference range, network density, and carrier sensing schemes. Related work on cross-layer optimization for FD multi-hop networks includes [17], [18], [19], [20], [21], [22]. In [17], Baranwal et al. derived expressions for the outage probability in a multi-hop FD network as a function of the average channel fading conditions and interference. Then the optimal number of multi-hop FD relay nodes is examined so as to minimize outage probability. In [18], Fang et al. proposed distributed algorithms to solve two multi-path routing problems (user profit maximization problem and network power consumption minimization problem) in a FD multi-hop wireless network. In [19], Mahboobi and Ardebilipour investigated a joint power allocation and routing problem for a single source destination pair in a FD multi-hop network. Under optimal routing, the weighted sum of power at relay nodes is minimized while the end-to-end link outage probability is kept below a threshold. In [20], Ramirez and Aazhang studied a joint routing and power allocation problem for a single source destination pair in a wireless FD network with imperfect self-interference cancellation. In [21], Yang and Shroff proposed a queue-length based CSMA-type scheduling algorithm for wireless networks with FD cut-through capability, where every node along the path of a traffic flow can receive and forward a packet simultaneously. In [22], Xie and Zhang showed an asymptotic analysis of network capacity under the protocol model for both HD and FD networks.

3 MODELING AND FORMULATION

In this section, we present mathematical modeling and formulation to study end-to-end session throughput maximization problem in a multi-hop wireless network. Each node is assumed to have FD capability. For comparison, we also present modeling with HD on each node in Section 5.1. Table 1 lists the notation used in this paper.

Consider a multi-hop wireless network with a set of nodes \mathcal{N} , where $N = |\mathcal{N}|$ is the number of nodes. We assume that each node in the network is equipped with a single antenna. Suppose that there is a set of \mathcal{F} active sessions in the network, with $F = |\mathcal{F}|$. Denote $s(f)$ and $d(f)$ as the source and destination nodes of session f , respectively,

TABLE 1
Notation

Symbol	Definition
\mathcal{N}	Set of nodes in the network
\mathcal{F}	Set of sessions in the network
T	Total number of time slots in a frame
\mathcal{L}	Set of links in the network
$\mathcal{L}_i^{\text{In}}$	The set of incoming links at node $i \in \mathcal{N}$
$\mathcal{L}_i^{\text{Out}}$	The set of outgoing links at node $i \in \mathcal{N}$
$x_l(t)$	A binary variable to indicate whether or not link l is active in time slot t
$c_l(t)$	Capacity of link l in time slot t
$u_l(t)$	SINR of link l in time slot t
$r_l(f)$	The data rate on link l that is attributed to session $f \in \mathcal{F}$
$r(f)$	The throughput of session $f \in \mathcal{F}$
P	Transmit power
G	A large constant
M	Number of line segments in linear approximation
$z_{lm}(t)$	A binary variable to indicate the specific segment m that $u_l(t)$ falls within in linear approximation
$\lambda_{lm}(t)$	Weight factor in linear approximation
$g_{(\text{Tx}(k), \text{Rx}(l))}$	Path attenuation loss from $\text{Tx}(k)$ to $\text{Rx}(l)$
$n_{\text{Rx}(l)}$	Ambient noise at node $\text{Rx}(l)$
W	Network bandwidth
β	The capability of self-interference cancellation
ϵ	Approximation error
$s(f)$	The source node of session $f \in \mathcal{F}$
$d(f)$	The destination node of session $f \in \mathcal{F}$

where $f \in \mathcal{F}$. For each session f , we assume the route from $s(f)$ to $d(f)$ is known *a priori*, which can be found by some routing algorithm (e.g., AODV [36], DSR [37]). For fairness in comparison, we employ the same routing for networks with FD or HD. This allows us to focus on the impact of scheduling.

Scheduling constraints. We assume time slot based scheduling, with T equal-length time slots in a frame. Within a time slot, a node may transmit and receive at the same time. When a node transmits, all the neighboring one-hop nodes will hear the signal. For unicast communication, among all the nodes that hear the signal, only one node belongs to the unicast session and will decode the signal. Consider a transmitter and its intended receiver as a (logical) link. Denote \mathcal{L} as the set of all possible links in the network and $x_l(t)$ as a binary variable to indicate whether or not link $l \in \mathcal{L}$ is active in time slot t , i.e., $x_l(t) = 1$ if link l is active and 0 otherwise. Then we have:

$$\sum_{l \in \mathcal{L}_i^{\text{Out}}} x_l(t) \leq 1, \quad (i \in \mathcal{N}, 1 \leq t \leq T), \quad (1)$$

$$\sum_{k \in \mathcal{L}_i^{\text{In}}} x_k(t) \leq 1, \quad (i \in \mathcal{N}, 1 \leq t \leq T), \quad (2)$$

where $\mathcal{L}_i^{\text{Out}}$ and $\mathcal{L}_i^{\text{In}}$ denote the sets of all possible outgoing and incoming links at node i , respectively.

Flow balance constraints. Denote $r(f)$ as the end-to-end throughput of session $f \in \mathcal{F}$ and $r_l(f)$ as the data rate on

link l that is attributed to session f . Then we have the following flow balance constraints. If node i is the source node of a session, then

$$\sum_{l \in \mathcal{L}_i^{\text{Out}}} r_l(f) = r(f), \quad (f \in \mathcal{F}, i = s(f)). \quad (3)$$

If node i is an intermediate relay node for session f , then

$$\sum_{k \in \mathcal{L}_i^{\text{In}}} r_k(f) = \sum_{l \in \mathcal{L}_i^{\text{Out}}} r_l(f), \quad (f \in \mathcal{F}, i \in \mathcal{N}, i \neq s(f), i \neq d(f)). \quad (4)$$

If node i is the destination node for session f , then

$$\sum_{k \in \mathcal{L}_i^{\text{In}}} r_k(f) = r(f), \quad (f \in \mathcal{F}, i = d(f)). \quad (5)$$

It can be easily verified that once (3) and (4) are satisfied, (5) is also satisfied. Therefore, it is sufficient to include (3) and (4) in the formulation.

Link rate constraints. Denote $c_l(t)$ as the achievable capacity of link l in time slot t . Then $c_l(t)$ can be calculated by Shannon's capacity formula by treating both mutual interference (from other links) and self interference (due to FD) as noise. Note that under FD, there is still non-negligible self interference that cannot be completely canceled [1]. It is therefore important to incorporate such remaining self-interference when calculating link capacity. For each transmit node, we assume that its transmit power is P when it is "on" (i.e., $x_l(t) = 1$) and 0 when it is "off". Denote $g_{(\text{Tx}(k), \text{Rx}(l))}$ as the path attenuation loss from transmit node of link k , $\text{Tx}(k)$, to receive node of link l , $\text{Rx}(l)$. Then we have,

$$c_l(t) = W \log_2 \left(1 + \frac{g_{(\text{Tx}(l), \text{Rx}(l))} \cdot P \cdot x_l(t)}{\sum_{k \in \mathcal{L}} g_{(\text{Tx}(k), \text{Rx}(l))} P x_k(t) + \sum_{m \in \mathcal{L}_i^{\text{Out}}} \beta P x_m(t) + n_{\text{Rx}(l)}} \right), \quad (6)$$

$(l \in \mathcal{L}, 1 \leq t \leq T),$

where W is the bandwidth. The first term in the denominator in (6) represents the interference signal power from other active links (mutual interference), the second term in the denominator represents residual self interference ($\text{Rx}(l)$ is transmitting on its outgoing link m), and $n_{\text{Rx}(l)}$ is the ambient noise at receive node $\text{Rx}(l)$. The value of β characterizes the performance of self-interference cancellation—the smaller the value of β , the cleaner the cancellation of self interference.

For $t = 1, 2, \dots, T$, the average link capacity is $\sum_{t=1}^T c_l(t)/T$. Since the sum of data rates over all sessions traversing a link cannot exceed the link's average capacity, We have

$$\sum_{f \in \mathcal{F}} r_l(f) \leq \frac{1}{T} \sum_{t=1}^T c_l(t), \quad (l \in \mathcal{L}). \quad (7)$$

Problem formulation. In this study, we are interested in end-to-end session throughput performance in a multi-hop network with FD at each node. Given that there are multiple

sessions in the network, we also need to consider fairness issue when maximizing throughput among competing sessions. Fairness can be defined in different ways. In this study, we choose the objective of maximizing the minimum throughput among all active sessions in the network (r_{\min}). This objective aims to achieve both throughput maximization and fairness among the sessions. The problem can be formulated as follows:

$$\begin{aligned} & \text{OPT-FD} \\ & \max \quad r_{\min} \\ & \text{s.t.} \quad r_{\min} \leq r(f) \quad (f \in \mathcal{F}); \\ & \quad \text{Scheduling constraints: (1), (2);} \\ & \quad \text{Flow balance constraints: (3), (4);} \\ & \quad \text{Link rate constraints: (6), (7).} \end{aligned}$$

In this formulation, W , $g_{(\text{Tx}(k), \text{Rx}(l))}$, β , $n_{\text{Rx}(l)}$ and P are constants; $c_l(t)$, $r(f)$ and $r_l(f)$ are continuous variables; and $x_k(t)$ is a binary variable. Note that constraints (6) are in the form of logarithmic functions and contain nonlinear terms inside the log functions. This optimization problem is in the form of a mixed-integer nonlinear program (MINLP), which is intractable. In the next section, we show how to linearize the nonlinear constraints in OPT-FD through reformulation and approximation.

4 PROBLEM REFORMULATION

In this section, we linearize the nonlinear constraints (6) in OPT-FD. Our roadmap is as follows. First, we employ *Reformulation-Linearization Technique* (RLT) [38, Chapter 6] to remove the nonlinear term (SINR) inside the logarithmic functions without loss of optimality. After this step, we obtain a reformulated problem OPT-FD_R. Then, we approximate the logarithmic functions in (6) with a set of linear constraints using *piece-wise linear approximation* technique. After these two steps, we obtain a linearized problem OPT-FD_L. We show that an optimal solution to OPT-FD_L is within $(1 - \varepsilon)$ -optimality of OPT-FD.

4.1 Reformulation of SINR Term

For (6), we replace the nonlinear SINR term inside the logarithmic function with a new variable $u_l(t)$. Then we obtain the following constraints:

$$c_l(t) = W \log_2(1 + u_l(t)), \quad (l \in \mathcal{L}, 1 \leq t \leq T), \quad (8)$$

$$u_l(t) = \frac{g_{(\text{Tx}(l), \text{Rx}(l))} P x_l(t)}{\sum_{k \in \mathcal{L}} g_{(\text{Tx}(k), \text{Rx}(l))} P x_k(t) + \sum_{m \in \mathcal{L}_{\text{Rx}(l)}^{\text{Out}}} \beta P x_m(t) + n_{\text{Rx}(l)}} \quad (l \in \mathcal{L}, 1 \leq t \leq T). \quad (9)$$

(9) can be re-written as:

$$\begin{aligned} & \sum_{k \in \mathcal{L}} g_{(\text{Tx}(k), \text{Rx}(l))} P x_k(t) u_l(t) + \sum_{m \in \mathcal{L}_{\text{Rx}(l)}^{\text{Out}}} \beta P x_m(t) u_l(t) + n_{\text{Rx}(l)} u_l(t) \\ & = g_{(\text{Tx}(l), \text{Rx}(l))} P x_l(t), \quad (l \in \mathcal{L}, 1 \leq t \leq T). \end{aligned} \quad (10)$$

Note that (10) has nonlinear terms $x_k(t)u_l(t)$ and $x_m(t)u_l(t)$. To remove these nonlinear terms, we employ RLT by introducing a new variable, $a_{kl}(t) = x_k(t)u_l(t)$.

Then (10) can be replaced by the following linear constraint:

$$\begin{aligned} & \sum_{k \in \mathcal{L}} g_{(\text{Tx}(k), \text{Rx}(l))} P a_{kl}(t) + \sum_{m \in \mathcal{L}_{\text{Rx}(l)}^{\text{Out}}} \beta P a_{mi}(t) + n_{\text{Rx}(l)} u_l(t) \\ & = g_{(\text{Tx}(l), \text{Rx}(l))} P x_l(t), \quad (l \in \mathcal{L}, 1 \leq t \leq T). \end{aligned} \quad (11)$$

Now we need to add constraints for $a_{kl}(t)$ and $a_{mi}(t)$. Denote G as an upper bound of $u_l(t)$ (SINR), which we can set to a large constant. Since $x_k(t)$ is a binary variable (therefore $0 \leq x_k(t) \leq 1$) and $0 \leq u_l(t) \leq G$, then the following constraints must hold:

$$[x_k(t) - 0] \cdot [u_l(t) - 0] \geq 0, \quad (l \in \mathcal{L}, k \in \mathcal{L}, 1 \leq t \leq T), \quad (12)$$

$$[x_k(t) - 0] \cdot [G - u_l(t)] \geq 0, \quad (l \in \mathcal{L}, k \in \mathcal{L}, 1 \leq t \leq T), \quad (13)$$

$$[1 - x_k(t)] \cdot [u_l(t) - 0] \geq 0, \quad (l \in \mathcal{L}, k \in \mathcal{L}, 1 \leq t \leq T), \quad (14)$$

$$[1 - x_k(t)] \cdot [G - u_l(t)] \geq 0, \quad (l \in \mathcal{L}, k \in \mathcal{L}, 1 \leq t \leq T). \quad (15)$$

Substituting $a_{kl}(t)$ for $x_k(t)u_l(t)$ in the above constraints, we obtain

$$a_{kl}(t) \geq 0, \quad (l \in \mathcal{L}, k \in \mathcal{L}, 1 \leq t \leq T), \quad (16)$$

$$G \cdot x_k(t) - a_{kl}(t) \geq 0, \quad (l \in \mathcal{L}, k \in \mathcal{L}, 1 \leq t \leq T), \quad (17)$$

$$u_l(t) - a_{kl}(t) \geq 0, \quad (l \in \mathcal{L}, k \in \mathcal{L}, 1 \leq t \leq T), \quad (18)$$

$$u_l(t) + G x_k(t) - a_{kl}(t) \leq G, \quad (l \in \mathcal{L}, k \in \mathcal{L}, 1 \leq t \leq T). \quad (19)$$

By adding the above new constraints for $a_{kl}(t)$, we have the following reformulated problem:

$$\begin{aligned} & \text{OPT-FD}_R \\ & \max \quad r_{\min} \\ & \text{s.t.} \quad r_{\min} \leq r(f) \quad (f \in \mathcal{F}); \\ & \quad \text{Scheduling constraints: (1), (2);} \\ & \quad \text{Flow balance constraints: (3), (4).} \\ & \quad \text{Link rate constraints: (7), (8), (11), (16)-(19).} \end{aligned}$$

Denote r^* and r_R^* as the optimal objective values of OPT-FD and OPT-FD_R, respectively. Then we have the following lemma:

Lemma 1. *The optimal objective values of OPT-FD and OPT-FD_R are identical, i.e., $r^* = r_R^*$.*

Proof. We show $r^* = r_R^*$ by two steps. First, we show that an optimal solution to OPT-FD can be mapped to a feasible solution to OPT-FD_R, that is, $r^* \leq r_R^*$ holds. Then, we show that an optimal solution to OPT-FD_R can also be mapped to a feasible solution to OPT-FD, that is, $r_R^* \leq r^*$ holds.

Step 1: In this step, we will show that $r^* \leq r_R^*$. We prove this inequality holds by showing that if r^* is an optimal objective value of OPT-FD, then it is an achievable objective value of OPT-FD_R. Suppose that r^* is an optimal objective value of OPT-FD, then there exists a solution $\psi = [r_{\min}, x_l(t), c_l(t), r_l(f), r(f)]$ that satisfies all

constraints in OPT-FD. Based on ψ , we can construct a solution $\hat{\psi}_R$ to OPT-FD_R as follows: $\hat{\psi}_R = [r_{\min}, x_l(t), u_l(t), c_l(t), r_l(f), r(f), a_{kl}(t)]$, where $u_l(t)$ is obtained by constraint (9) and $a_{kl}(t) = x_k(t)u_l(t)$. We now show that the constructed solution $\hat{\psi}_R$ is a feasible solution to OPT-FD_R. Since ψ satisfies constraints (1)-(4) and (7) in OPT-FD, it is obvious that $\hat{\psi}_R$ also satisfies these constraints in OPT-FD_R. Since ψ satisfies constraint (6) in OPT-FD, it is easy to verify that $\hat{\psi}_R$ satisfies constraint (8) and (11) in OPT-FD_R. Since $x_k(t)$ is a binary variable and $0 \leq u_l(t) \leq G$, then $a_{kl}(t) = 0$ when $x_k(t) = 0$, and $a_{kl}(t) = u_l(t)$ when $x_k(t) = 1$. Therefore, it is easy to verify that $\hat{\psi}_R$ satisfies constraints (16)-(19). Since $\hat{\psi}_R$ satisfies all constraints in OPT-FD_R, it is a feasible solution to OPT-FD_R. Note that the objective function in OPT-FD_R is the same as in OPT-FD, therefore, the feasible objective value corresponding to solution $\hat{\psi}_R$ is equal to r^* . Since OPT-FD_R is a maximization problem and its optimal objective value is r_R^* , then $r^* \leq r_R^*$ holds.

Step 2: In this step, we show that $r_R^* \leq r^*$. We show this inequality holds by arguing that if r_R^* is an optimal objective value of OPT-FD_R, then it is also an achievable objective value of OPT-FD. Suppose that r_R^* is an optimal objective value of OPT-FD_R. Then there exists a solution $\psi_R = [r_{\min}, x_l(t), u_l(t), c_l(t), r_l(f), r(f), a_{kl}(t)]$ that satisfies all constraints in OPT-FD_R. Based on ψ_R , we can construct a solution $\hat{\psi}$ to OPT-FD as follows: $\hat{\psi} = [r_{\min}, x_l(t), c_l(t), r_l(f), r(f)]$. We now show that the constructed solution $\hat{\psi}$ is a feasible solution to OPT-FD. Since ψ_R satisfies constraints (1)-(4) and (7) in OPT-FD_R, it is obvious that $\hat{\psi}$ also satisfies these constraints in OPT-FD. Now we show that since ψ_R satisfies constraints (8), (11), and (16)-(19) in OPT-FD_R, then $\hat{\psi}$ satisfies constraint (6) in OPT-FD. Note that constraint (6) in OPT-FD is identical to constraints (8) and (9) in OPT-FD_R, then constraint (9) is replaced by constraints (11) and (16)-(19). Now we prove that once ψ_R satisfies constraints (11) and (16)-(19), it also satisfies constraint (9) by showing that $a_{kl}(t) = x_k(t)u_l(t)$ holds. Since $x_k(t)$ is a binary variable, according to constraints (16)-(19), $a_{kl}(t) = 0$ when $x_k(t) = 0$ and $a_{kl}(t) = u_l(t)$ when $x_k(t) = 1$, which indicates that $a_{kl}(t) = x_k(t)u_l(t)$ holds. Therefore, $\hat{\psi}$ satisfies constraint (6) in OPT-FD. Since $\hat{\psi}$ satisfies all constraints in OPT-FD, it is a feasible solution to OPT-FD and its corresponding objective value equals to r_R^* . Since r^* is the optimal objective value of OPT-FD, $r_R^* \leq r^*$ holds. This completes the proof. \square

4.2 Piece-Wise Linear Approximation of Log Function

In OPT-FD_R, (8) is in the form of a logarithmic function. To linearize this logarithmic function, we employ *piece-wise linear approximation* technique. The idea is to use a finite number (say M) of line segments to approximate the logarithmic function, as shown in Fig. 1. First, we determine the range for $u_l(t)$. Denote U_l^{\min} and U_l^{\max} as the lower and upper bounds of $u_l(t)$ when link l is active ($x_l(t) = 1$), respectively. Then one lower bound could be that all interfering links are active at the same time, i.e.,

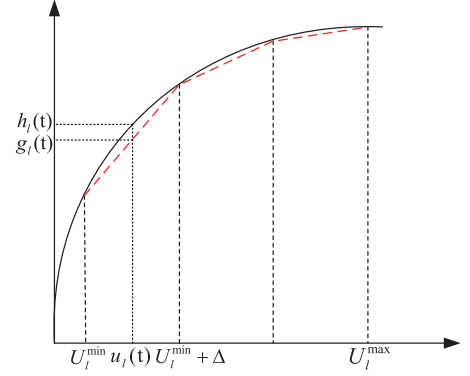


Fig. 1. An illustration of piecewise linear approximation (with $M = 3$) for $h_l(t) = \log_2(1 + u_l(t))$.

$U_l^{\min} = \frac{g(\text{Tx}(l), \text{Rx}(l))^P}{\sum_{k \in \mathcal{L}} g(\text{Tx}(k), \text{Rx}(l))^P + \sum_{m \in \mathcal{L}^{\text{Out}}} \beta P + n_{\text{Rx}(l)}}$. Likewise, an upper bound could be that all interfering links (except l) are inactive at the same time, i.e., $U_l^{\max} = \frac{g(\text{Tx}(l), \text{Rx}(l))^P}{n_{\text{Rx}(l)}}$. Then, for $h_l(t) = \log_2(1 + u_l(t))$, we construct a piecewise linear approximation $g_l(t)$ by connecting points $(U_l^{\min} + m\Delta, \log_2(1 + U_l^{\min} + m\Delta))$, where $\Delta = \frac{U_l^{\max} - U_l^{\min}}{M}$ and $m = 0, 1, \dots, M$. We will determine the value of M to achieve the desired accuracy in Lemma 3.

Suppose $u_l(t)$ is within the m th segment between (U_l^{\min}, U_l^{\max}) , i.e., $u_l(t) \in [U_l^{\min} + (m-1)\Delta, U_l^{\min} + m\Delta]$, then $u_l(t)$ can be represented by

$$u_l(t) = \lambda_{l,m-1}(t)[U_l^{\min} + (m-1)\Delta] + \lambda_{lm}(t)(U_l^{\min} + m\Delta), \quad (20)$$

where $\lambda_{l,m-1}(t)$ and $\lambda_{lm}(t)$ are two weights and satisfy:

$$\lambda_{l,m-1}(t) + \lambda_{lm}(t) = 1, \quad (\lambda_{l,m-1}(t) \geq 0, \lambda_{lm}(t) \geq 0). \quad (21)$$

With $u_l(t)$ in (20), its corresponding $g_l(t)$ value is:

$$g_l(t) = \lambda_{l,m-1}(t) \log_2(1 + U_l^{\min} + (m-1)\Delta) + \lambda_{lm}(t) \log_2(1 + U_l^{\min} + m\Delta). \quad (22)$$

Note that (20) to (22) are for a given m th segment, $m = 1, 2, \dots, M$. Now we extend the representation to the entire piecewise linear curve. First we need to find out the position of $u_l(t)$. We use a binary variable $z_{lm}(t)$, $1 \leq m \leq M$ to represent the specific segment that $u_l(t)$ falls within. If $u_l(t)$ falls within the m th segment (i.e., $U_l^{\min} + (m-1)\Delta \leq u_l(t) \leq U_l^{\min} + m\Delta$), then $z_{lm}(t) = 1$; otherwise, $z_{lm}(t) = 0$. Recall that $u_l(t)$ represents the SINR of link l . When link l is inactive (i.e., $x_l(t) = 0$), $u_l(t)$ is 0 and does not fall in any of the M segments (see Fig. 1). Therefore, all of the $z_{lm}(t)$ value should be 0. When link l is active (i.e., $x_l(t) = 1$), $u_l(t)$ can only fall in one of the m segments, we have

$$\sum_{m=1}^M z_{lm}(t) = x_l(t), \quad (l \in \mathcal{L}, 1 \leq t \leq T). \quad (23)$$

Based on (20) and (21), when $u_l(t)$ falls within the m th segment, we can only have $\lambda_{l,m-1}(t)$ and $\lambda_{lm}(t)$ be positive

and all other $\lambda_{lk}(t)$ be zero ($k \neq m-1, k \neq m$). That is, if $\lambda_{l0}(t) > 0$ then $z_{l1} = 1$. Since $\lambda_{l0}(t) \in [0, 1]$ and z_{l1} is a binary indicator, we have

$$\lambda_{l0}(t) \leq z_{l1}(t), \quad (l \in \mathcal{L}, 1 \leq t \leq T). \quad (24)$$

Likewise, if $\lambda_{lm}(t) > 0$, then $z_{lm} = 1$ or $z_{l,m+1} = 1$, $1 \leq m < M$. We have

$$\lambda_{lm}(t) \leq z_{lm}(t) + z_{l,m+1}(t), \quad (l \in \mathcal{L}, 1 \leq t \leq T, 1 \leq m \leq M-1). \quad (25)$$

Finally, if $\lambda_{lM}(t) > 0$, then $z_{lM} = 1$. We have

$$\lambda_{lM}(t) \leq z_{lM}(t), \quad (l \in \mathcal{L}, 1 \leq t \leq T). \quad (26)$$

The above three constraints ensure that there are at most two adjacent positive $\lambda_{lm}(t)$, $m = 0, 1, \dots, M$ for each $u_l(t)$. Now (20) to (22) can be rewritten for the entire piecewise curve as follows:

$$u_l(t) = \sum_{m=0}^M \lambda_{lm}(t)(U_l^{\min} + m\Delta), \quad (l \in \mathcal{L}, 1 \leq t \leq T), \quad (27)$$

where $\lambda_{lm}(t)$ satisfies:

$$\sum_{m=0}^M \lambda_{lm}(t) = x_l(t), \quad (l \in \mathcal{L}, 1 \leq t \leq T), \quad (28)$$

$$g_l(t) = \sum_{m=0}^M \lambda_{lm}(t) \log_2(1 + U_l^{\min} + m\Delta), \quad (l \in \mathcal{L}, 1 \leq t \leq T). \quad (29)$$

The following lemma characterizes the approximation error ratio $\frac{h_l(t) - g_l(t)}{h_l(t)}$ as a function of M .

Lemma 2. For a given $u_l(t)$, $l \in \mathcal{L}$, the ratio of linear approximation error $\frac{h_l(t) - g_l(t)}{h_l(t)}$ is upper bounded by $\frac{U_l^{\max} - U_l^{\min}}{M \cdot \ln(2) \cdot (1 + U_l^{\min}) \log_2(1 + U_l^{\min})}$.

Proof. Since the logarithm function $h_l(t)$ becomes closer to linear as the value of $u_l(t)$ increases, the maximum approximation error occurs within the first line segment, i.e., $u_l(t) \in [U_l^{\min}, U_l^{\min} + \Delta]$. Denote K as the gradient of logarithm function at U_l^{\min} . Then we have $K = \frac{1}{\ln(2)(1 + U_l^{\min})}$. Denote E_{\max} as the maximum approximation error in the entire range $[U_l^{\min}, U_l^{\max}]$. Denote \mathcal{R} as $[U_l^{\min}, U_l^{\min} + \Delta]$. Since the maximum approximation error occurs within the first line segment, we have

$$\begin{aligned} E_{\max} &= \max_{u_l(t) \in \mathcal{R}} \frac{h_l(t) - g_l(t)}{h_l(t)} \\ &\leq \frac{\max_{u_l(t) \in \mathcal{R}} \{h_l(t) - g_l(t)\}}{\min_{u_l(t) \in \mathcal{R}} \{h_l(t)\}} \\ &\leq \frac{K\Delta}{\min_{u_l(t) \in \mathcal{R}} \{h_l(t)\}} \\ &\leq \frac{K\Delta}{\log_2(1 + U_l^{\min})} \\ &= \frac{U_l^{\max} - U_l^{\min}}{M \cdot \ln(2) \cdot (1 + U_l^{\min}) \log_2(1 + U_l^{\min})}, \end{aligned}$$

where the last equation follows from the fact that $\Delta = \frac{U_l^{\max} - U_l^{\min}}{M}$ and $K = \frac{1}{\ln(2)(1 + U_l^{\min})}$. \square

Replacing $c_l(t)$ in (8), which is a logarithm function, with its piecewise linear approximation ($W \cdot g_l(t)$), we have:

$$c_l(t) = W \cdot \sum_{m=0}^M \lambda_{lm}(t) \log_2(1 + U_l^{\min} + m\Delta), \quad (l \in \mathcal{L}, 1 \leq t \leq T). \quad (30)$$

With the piecewise linear approximation for $c_l(t)$, we have the following linear formulation:

OPT-FD_L

$$\begin{aligned} \max \quad & r_{\min} \\ \text{s.t} \quad & r_{\min} \leq r(f) \quad (f \in \mathcal{F}); \\ & \text{Scheduling constraints: (1), (2);} \\ & \text{Flow balance constraints: (3), (4);} \\ & \text{Link rate constraints:} \\ & (7), (11), (16)-(19); (23)-(28); (30). \end{aligned}$$

In this formulation, W , G , $g_{(\text{Tx}(k), \text{Rx}(l))}$, β , $n_{\text{Rx}(l)}$, P , M , U_l^{\min} and U_l^{\max} are constants; $x_l(t)$ and $z_{lm}(t)$ are integer variables; and $c_l(t)$, $r_l(f)$, $r(f)$, $u_l(t)$, $a_{kl}(t)$ and $\lambda_{lm}(t)$ are continuous variables. The optimization problem is in the form of a mixed-integer linear program (MILP). The theoretical worst-case complexity of solving a general MILP problem is exponential [39]. There exists highly efficient optimal algorithms (e.g., branch-and-bound [38, Chapter 5]) and heuristic algorithms (e.g., sequential fixing algorithm [38, Chapter 10]). For most practical-sized networks, a commercial solver such as CPLEX [40] may also be effective. Since the goal of this paper is to explore the performance limit of FD multi-hop network, we will employ CPLEX to solve OPT-FD_L.

The linear approximation error in Lemma 2 can be made arbitrarily small when we increase the number of linear segments M . Denote r_L^* as the optimal objective value of OPT-FD_L. Then the following lemma specifies the value of M so that r_L^* is within $(1 - \epsilon)$ of r^* , the objective value of OPT-FD.

Lemma 3. For a given performance gap ϵ , $0 < \epsilon \ll 1$, if $M = \lceil \frac{U_l^{\max} - U_l^{\min}}{\epsilon \cdot \ln(2) \cdot (1 + U_l^{\min}) \log_2(1 + U_l^{\min})} \rceil$, then we have $(1 - \epsilon)r^* \leq r_L^* \leq r^*$.

Proof. We prove this lemma by two steps. First, we show that $(1 - \epsilon)r^* \leq r_L^*$ holds. Since r^* is the optimal objective value of OPT-FD, its corresponding solution $\psi = [x_l(t), c_l(t), r_l(f), r(f)]$ is clearly a feasible solution and satisfies all constraints in OPT-FD. Based on ψ , we can construct $\hat{\psi}_L = [x_l(t), u_l(t), \hat{c}_l(t), (1 - \epsilon)r_l(f), (1 - \epsilon)r(f), a_{kl}(t), z_{lm}(t), \lambda_{lm}(t)]$. It can be verified that $\hat{\psi}_L$ is a feasible solution to OPT-FD_L and its corresponding objective value is $(1 - \epsilon)r^*$. Since OPT-FD_L is a maximization problem, its optimal objective value r_L^* must be greater or equal to its feasible objective value $(1 - \epsilon)r^*$. Therefore, $(1 - \epsilon)r^* \leq r_L^*$ holds. Following the same token, we can show that $r_L^* \leq r^*$ holds.

Step 1: In this step, we will show that $(1 - \epsilon)r^* \leq r_L^*$. We prove this inequality holds by showing that if r^* is an optimal objective value of OPT-FD, then $(1 - \epsilon)r^*$ is an achievable objective value of OPT-FD_L. Suppose that r^* is an optimal objective value of OPT-FD. Then there exists a solution $\psi = [x_l(t), c_l(t), r_l(f), r(f)]$ that satisfies all

constraints in OPT-FD. Based on ψ , we can construct a solution ψ_R to OPT-FD_R as follows: $\psi_R = [x_l(t), u_l(t), c_l(t), r_l(f), r(f), a_{kl}(t)]$, where $u_l(t)$ is obtained by constraint (9) and $a_{kl}(t) = x_k(t)u_l(t)$. Based on Lemma 1, we know that its corresponding objective value is equal to r^* . Then based on ψ_R , we can construct a solution $\hat{\psi}_L$ to OPT-FD_L as follows: $\hat{\psi}_L = [x_l(t), u_l(t), \hat{c}_l(t), (1 - \epsilon)r_l(f), (1 - \epsilon)r(f), a_{kl}(t), z_{lm}(t), \lambda_{lm}(t)]$.

We now show that the constructed solution $\hat{\psi}_L$ is a feasible solution to OPT-FD_L. For any given $u_l(t)$, we can always find $z_{lm}(t)$, $\lambda_{lm}(t)$ and $\hat{c}_l(t)$ by constraints (23)-(28) and (30). Since ψ_R satisfies constraints (1)-(4), (11), and (16)-(19) in OPT-FD_R, it is easy to verify that $\hat{\psi}_L$ also satisfies these constraints in OPT-FD_L. Based on Lemma 2, we know that we can find a M so that $\hat{c}_l(t) \geq (1 - \epsilon)c_l(t)$.

The corresponding $M = \lceil \frac{U_l^{\max} - U_l^{\min}}{\epsilon \cdot \ln 2 \cdot (1 + U_l^{\min}) \log_2(1 + U_l^{\min})} \rceil$. Therefore, $\hat{\psi}_L$ satisfies constraint (7). Since $\hat{\psi}_L$ satisfies all constraints in OPT-FD_L, it is a feasible solution to OPT-FD_L. Since the objective function is a linear function of $r(f)$ in both OPT-FD and OPT-FD_L, we know that the feasible objective value of OPT-FD_L corresponding to solution $\hat{\psi}_L$ is $(1 - \epsilon)r^*$. Since OPT-FD_L is a maximization problem and its optimal objective value is r_L^* , $r_L^* \geq (1 - \epsilon)r^*$ holds.

Step 2: In this step, we show that $r_L^* \leq r^*$. We show this inequality holds by arguing that if r_L^* is an optimal objective value of OPT-FD_L, then r_L^* is also an achievable objective value of OPT-FD. Suppose that r_L^* is an optimal objective value of OPT-FD_L. Then there exists a solution $\psi_L = [x_l(t), u_l(t), \tilde{c}_l(t), r_l(f), r(f), a_{kl}(t), z_{lm}(t), \lambda_{lm}(t)]$ that satisfies all constraints in OPT-FD_L. Based on ψ_L , we can construct a solution $\hat{\psi}_R$ to OPT-FD_R as follows: $\hat{\psi}_R = [x_l(t), u_l(t), c_l(t), r_l(f), r(f), a_{kl}(t)]$, where $c_l(t)$ is obtained by constraint (8).

We now show that the constructed solution $\hat{\psi}_R$ is a feasible solution to OPT-FD_R. Since ψ_L satisfies constraints (1)-(4), (11) and (16)-(19) in OPT-FD_L, it is not difficult to see that $\hat{\psi}_R$ also satisfies these constraints in OPT-FD_R. Based on Lemma 2, we know that the relationship between $c_l(t)$ and its piecewise linear approximation $\tilde{c}_l(t)$ is that $c_l(t) \geq \tilde{c}_l(t)$. Therefore, $\hat{\psi}_R$ satisfies constraint (7). Since $\hat{\psi}_R$ satisfies all constraints in OPT-FD_R, it is a feasible solution to OPT-FD_R and its corresponding objective value equals to r_L^* . Based on $\hat{\psi}_R$, we can construct a solution $\hat{\psi} = [x_l(t), c_l(t), r_l(f), r(f)]$. Based on lemma 1, it is easy to see that $\hat{\psi}$ is a feasible solution to OPT-FD and its corresponding objective value equals to r_L^* . Since r^* is the optimal objective value of OPT-FD, $r_L^* \leq r^*$ holds. This completes the proof. \square

5 NUMERICAL INVESTIGATION

In this section, we conduct numerical study to compare end-to-end session throughput performance between FD and HD in multi-hop wireless networks. Our results show that the throughput ratio of FD over HD exceeds 2 in many cases. We also give insights on why $2\times$ is not the fundamental performance barrier for network level throughput.

5.1 Half Duplex Model

For comparison, we present mathematical modeling for a multi-hop wireless network with HD capability on each node. It is easy to see that constraints (3), (4) and (7) from OPT-FD still apply to HD network. But there are some new constraints for HD.

Half duplex constraints. Under HD, in one time slot, a node can operate in only one mode (transmit, receive, idle). Then we have

$$\sum_{k \in \mathcal{L}_i^{\text{In}}} x_k(t) + \sum_{l \in \mathcal{L}_i^{\text{Out}}} x_l(t) \leq 1, \quad (i \in \mathcal{N}, 1 \leq t \leq T). \quad (31)$$

Link rate constraints. The achievable capacity on link l can be calculated using Shannon's capacity formula by considering only the mutual interference (from other links). We have

$$c_l(t) = W \log_2 \left(1 + \frac{g_{(\text{Tx}(l), \text{Rx}(l))} \cdot P \cdot x_l(t)}{\sum_{k \in \mathcal{L}} g_{(\text{Tx}(k), \text{Rx}(l))} P x_k(t) + n_{\text{Rx}(l)}} \right), \quad (l \in \mathcal{L}, 1 \leq t \leq T). \quad (32)$$

5.2 Simulation Setting

We consider a 30-node multi-hop wireless network, with nodes randomly deployed in a 100 m \times 100 m area. The bandwidth is normalized to one unit (i.e., $W = 1$). The transmission power of each node is set to $P = 20$ dBm. The path loss parameter $g_{(\text{Tx}(k), \text{Rx}(l))} = [20 \log_{10}(d) + 38.25]$ (in dB) [41], where d is the distance between nodes $\text{Tx}(k)$ and $\text{Rx}(l)$. We assume the self-interference cancellation parameter $\beta = 110$ dB [1] and ambient noise $n_{\text{Rx}(l)} = -90$ dBm. The number of time slots in a frame is $T = 4$. We set $\epsilon = 5\%$, which guarantees that the obtained solution is within 5 percent from the optimum.

5.3 An Example

For the 30-node network instance in Fig. 2, we increase the number of sessions from 1 to 9. The source node and destination node of each session are randomly selected, with the route between the two being the shortest path route. Fig. 3a shows the achievable throughput for all sessions in both FD and HD networks as the number of sessions grows. Note that the achievable throughput decreases (down to 0) under both FD and HD when the number of sessions increases. But for the same number of sessions, the objective value under FD is higher than that under HD. Fig. 3b shows the ratio between the achievable throughput for FD and HD. When the number of sessions are 1, 2, 3, and 4, the ratios are 1.41, 1.45, 3.51 and 3.14, showing that FD can indeed exceed the $2\times$ performance barrier in a multi-hop network. When the number of session is 5, the throughput of HD network goes to zero, indicating that the schedulable region of HD network cannot support these five sessions (Fig. 2e). In this case, there are three sessions intersect at node N_2 , with three incoming links ($N_9 \rightarrow N_2$, $N_{20} \rightarrow N_2$, $N_{25} \rightarrow N_2$) and three outgoing links ($N_2 \rightarrow N_1$, $N_2 \rightarrow N_3$, $N_2 \rightarrow N_{11}$). Since there are only four time slots in the system, HD network cannot find a feasible scheduling solution and thus renders an objective value of 0. For FD, it can offer a positive throughput until there are nine sessions in the network (Fig. 2i). When there are nine sessions, five sessions intersect at node

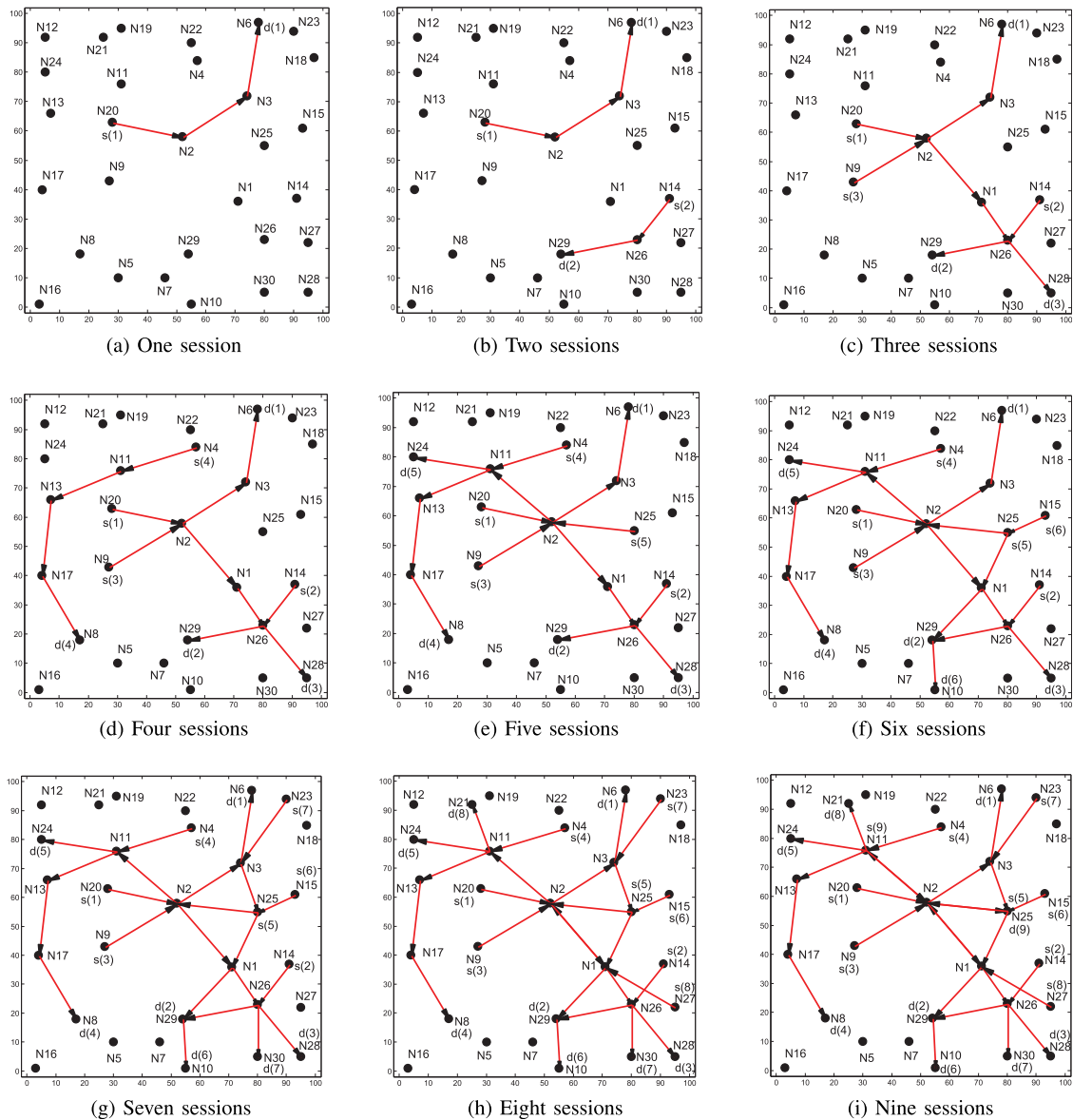


Fig. 2. A 30-node network instance. The number of sessions in the network increases from 1 to 9.

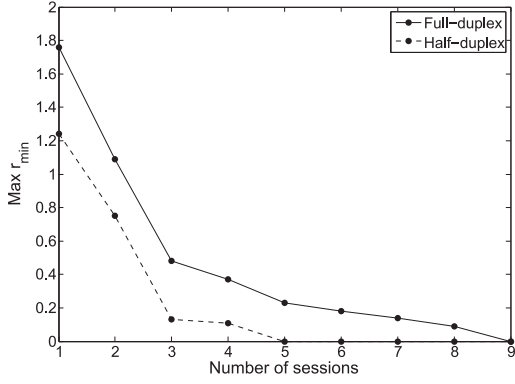
N_2 . With five incoming links ($N_1 \rightarrow N_2$, $N_9 \rightarrow N_2$, $N_{11} \rightarrow N_2$, $N_{20} \rightarrow N_2$, $N_{25} \rightarrow N_2$) and four outgoing links ($N_2 \rightarrow N_1$, $N_2 \rightarrow N_3$, $N_2 \rightarrow N_{11}$, $N_2 \rightarrow N_{25}$) at node N_2 , this is beyond what can be scheduled with 4 time slots.

When the number of time slots increases (e.g., six or more), the schedulable regions for both FD and HD will increase. But the general shape for achievable throughput under both remains the same as that in Fig. 3a, except that each curve intersects the x -axis with a higher session number. To better illustrate the idea, we increase the number of time slots to 6 for the same network instance. Fig. 4a shows the achievable throughput for all sessions in both FD and HD networks as the number of sessions grows. Compared with Fig. 3a, the general shape for achievable throughput remains the same, except that the schedulable regions for HD and FD increase from 4 to 7 and 8 to 10, respectively. Note that when there are four time slots, the schedulable region of HD network cannot support the five sessions in Fig. 2e since there are six links involving node N_2 . When the number of time slots is increased to 6, HD network can find a

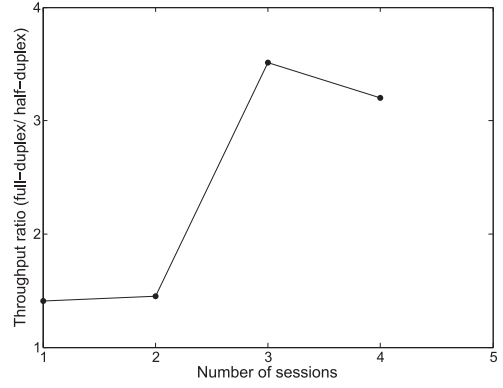
feasible scheduling solution among these six links and therefore has a positive throughput as shown in Fig. 4a. When there are eight sessions, the throughput of HD network goes to zero, indicating that the schedulable region of HD network cannot support these eight sessions with six time slots. In this case, there are four sessions intersect at node N_2 , with four incoming links ($N_1 \rightarrow N_2$, $N_9 \rightarrow N_2$, $N_{20} \rightarrow N_2$, $N_{25} \rightarrow N_2$) and three outgoing links ($N_2 \rightarrow N_1$, $N_2 \rightarrow N_3$, $N_2 \rightarrow N_{11}$) (Fig. 2h). Since there are six time slots in the system, HD network cannot find a feasible scheduling solution among these seven links and thus renders an objective value of 0. For FD, it can offer a positive throughput until there are 11 sessions in the network. Fig. 4b shows the ratio between the achievable throughput for FD and HD. When there are five and six sessions in the network, the ratio between achievable throughput of FD and HD exceeds 2.

5.4 A Closer Look Under the Hood

To see why $2\times$ is not a fundamental limit, let's take a closer look at the network instance in the last section when there are

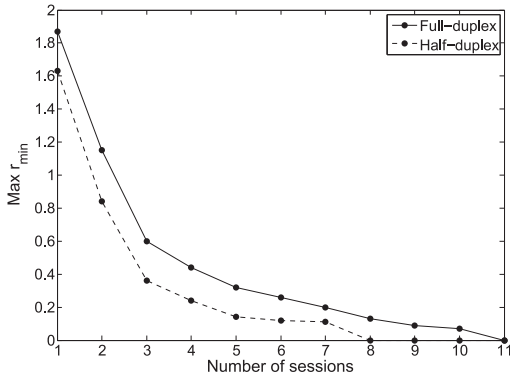


(a) Achievable throughput under FD and HD for a 30-node network as the number of sessions increases.

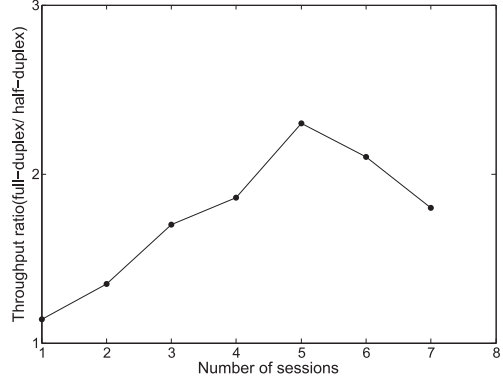


(b) Ratio between achievable throughput of FD and HD for a 30-node network as the number of sessions increases.

Fig. 3. Throughput performance in a 30-node network with increasing number of sessions under FD and HD when $T = 4$ time slots.

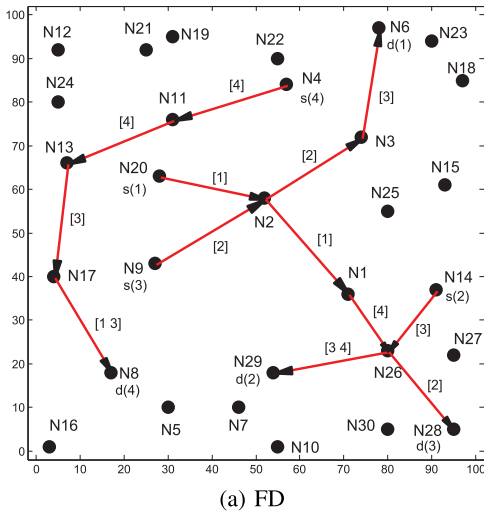


(a) Achievable throughput under FD and HD for a 30-node network as the number of sessions increases.

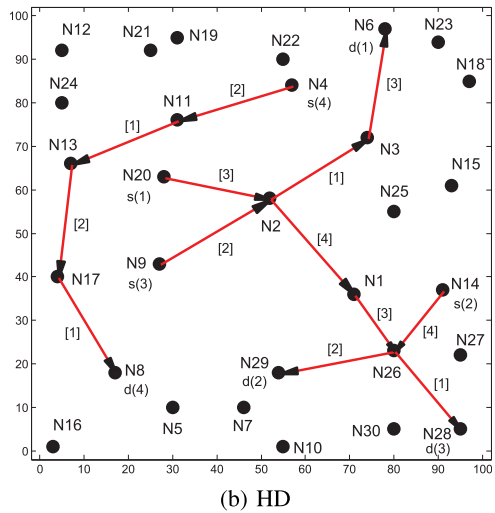


(b) Ratio between achievable throughput of FD and HD for a 30-node network as the number of sessions increases.

Fig. 4. Throughput performance in a 30-node network with increasing number of sessions under FD and HD when $T = 6$ time slots.



(a) FD



(b) HD

Fig. 5. Link scheduling for a 30-node network with four sessions: (a) FD and (b) HD.

four sessions (Fig. 2d) in the network and $T = 4$ time slots. Figs. 5a and 5b show the details of link scheduling for FD and HD, respectively. In both figures, $s(f)$ and $d(f)$ denote the source and destination nodes for session f , respectively. The number inside the bracket next to each link represents the time slot in which the link is active. Table 2 lists the scheduling details of each link, including the time slots in which it is

active, the corresponding link capacity, and the average link capacity over $T (= 4)$ time slots (i.e., $\frac{1}{T} \sum_{t=1}^T c_l(t)$).

We discuss HD and FD cases separately.

- *HD*. The achievable throughput of HD from our solution is 0.117. In Table 2, this shows that link $(N_9 \rightarrow N_2)$ is the bottleneck link, which has an average

TABLE 2
Details of Link Scheduling Under FD and HD
for a 30-Node Network with Four Sessions

Link	FD		HD	
	(Time Slot, Link Capacity)	Average Link Capacity	(Time Slot, Link Capacity)	Average Link Capacity
$(N_{20} \rightarrow N_2)$	(1, 2.252)	0.563	(3, 0.598)	0.149
$(N_2 \rightarrow N_3)$	(2, 1.498)	0.375	(1, 0.572)	0.143
$(N_3 \rightarrow N_6)$	(3, 1.555)	0.389	(3, 1.579)	0.395
$(N_{14} \rightarrow N_{26})$	(3, 2.603)	0.651	(4, 2.728)	0.682
$(N_{26} \rightarrow N_{29})$	(3, 0.628) (4, 1.151)	0.445	(2, 1.075)	0.269
$(N_9 \rightarrow N_2)$	(2, 1.471)	0.368	(2, 0.468)	0.117
$(N_2 \rightarrow N_1)$	(1, 1.616)	0.404	(4, 0.697)	0.174
$(N_1 \rightarrow N_{26})$	(4, 2.907)	0.727	(3, 2.527)	0.632
$(N_{26} \rightarrow N_{28})$	(2, 2.349)	0.587	(1, 2.701)	0.675
$(N_4 \rightarrow N_{11})$	(4, 2.019)	0.505	(2, 0.717)	0.179
$(N_{11} \rightarrow N_{13})$	(4, 1.641)	0.410	(1, 1.087)	0.271
$(N_{13} \rightarrow N_{17})$	(3, 1.732)	0.433	(2, 1.026)	0.257
$(N_{17} \rightarrow N_8)$	(1, 1.157) (3, 1.454)	0.653	(1, 1.485)	0.371

throughput of 0.117. In Fig. 5b, we see that link $(N_9 \rightarrow N_2)$ is active in time slot 2. Also in time slot 2, three links $(N_4 \rightarrow N_{11}, N_{13} \rightarrow N_{17}, \text{ and } N_{26} \rightarrow N_{29})$ are also active and their transmitters produce strong interference to N_2 . On the other hand, at node N_2 , it has two incoming links and two outgoing links (for sessions 1 and 3). Due to HD, all four time slots are used by the four links involving N_2 and there is no extra time slot for bottleneck link $(N_9 \rightarrow N_2)$.

- *FD*. On the other hand, the achievable throughput of FD is 0.368. In Table 2, this shows that link $(N_9 \rightarrow N_2)$ is again the bottleneck link, which has an average throughput of 0.368. In Fig. 5a, link $(N_9 \rightarrow N_2)$ and $(N_2 \rightarrow N_3)$ are both active in time slot 2 (due to FD at N_2). Except for these two links, only link $(N_{26} \rightarrow N_{28})$ is scheduled to be active in time slot 2. Therefore, there is only one interfering link for link $(N_9 \rightarrow N_2)$. Note that such scheduling solution is infeasible under HD. It exploits FD capability to reduce the number of interfering links for bottleneck link $(N_9 \rightarrow N_2)$ to the minimum. Therefore, the throughput on link $(N_9 \rightarrow N_2)$ in FD can be much higher than in HD. In fact, the ratio between the achievable throughput of FD and HD is $0.368/0.117 = 3.14$, exceeding the $2\times$ barrier.

In Section 4.2, we employ *piece-wise linear approximation* technique to linearize the link capacity constraint (8). Now we present the approximation error between the original objective values and the approximated objective values. Table 3 lists the optimal objective values of the original problem (denoted as r^*) and linearized problem (denoted as r_L^*), and the normalized approximation error (i.e., $\frac{r^* - r_L^*}{r^*}$) for both FD and HD networks. It shows that the actual approximation errors in the case study are smaller than the target approximation error ($\epsilon = 5\%$). Therefore, the piece-wise

TABLE 3
Approximation Error between Optimal Objective Values
of Original Problem and Linearized Problem

Network Type	Objective Value of Original Problem	Objective Value of Linearized Problem	Approximation Error
FD	0.374	0.368	0.017
HD	0.120	0.117	0.025

linear approximation technique used in our paper can indeed guarantee that the obtained objective value is within 5 percent from the optimum.

In summary, for end-to-end throughput of a session in a multi-hop wireless network, the advantage of FD is not limited to achieving simultaneous transmission and reception at each node. Rather, as shown in this case study, FD capability allows a much larger solution space for scheduling. Since a session's throughput at the network level is determined by the capacity of the bottleneck link along its path, a larger scheduling space will help to increase the bottleneck link rate by reducing the number of interfering links in the network. Therefore, for end-to-end throughput of a session, its throughput ratio under FD over that under HD is no longer limited by 2, as in the case for a single FD node in isolation.

5.5 Additional Results

The results in Section 5.3 are from one 30-node network instance with $T = 4$ time slots for increasing number of sessions. Now we perform the same study for 100 randomly generated 30-node network instances with $T = 4$ time slots. For each instance, we increase the number of sessions from 1 to 8.

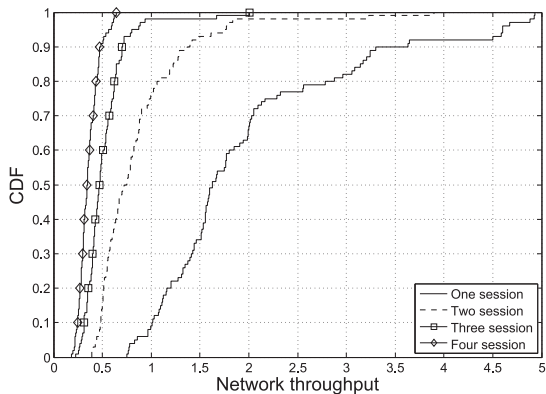
Figs. 6 and 7 present the general trend of achievable throughput as the number of sessions increases from 1 to 8 under FD and HD, respectively. In both figures, we show the relative ordering relationship among the CDF curves (from 100 instances) for different number of sessions. In the case when the throughput is zero, it shows that we will have higher probability of zero throughput as the number of session increases, indicating an increasing level of difficulty to schedule the sessions with non-zero throughput.

Table 4 shows the distribution of throughput ratio between FD and HD for 100 network instances as the number of sessions increases from 1 to 8. As shown in the third column, when the number of sessions increases from 2 to 8, there are 8, 27, 44, 52, 60, 66, and 71 instances that achieve a throughput ratio ≥ 2 .

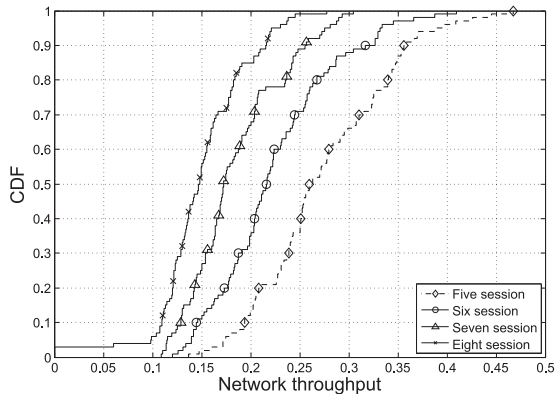
Fig. 8 presents the ratio between the average achievable throughput of FD and HD (over 100 network instances) as the number of sessions increases from 1 to 8. It shows that the ratio between average throughput of FD and HD becomes more significant as the number of sessions increases.

5.6 Impact of Various System Parameters

In Section 5.4, we present the solution details for a 30-node network instance. In Section 5.5, we perform numerical study for 100 randomly generated 30-node network instances. Through these results, we show that the achievable session throughput in a FD network can exceed $2\times$ of that in a HD network in many cases. To show the robustness of our results, we further perform numerical study under different

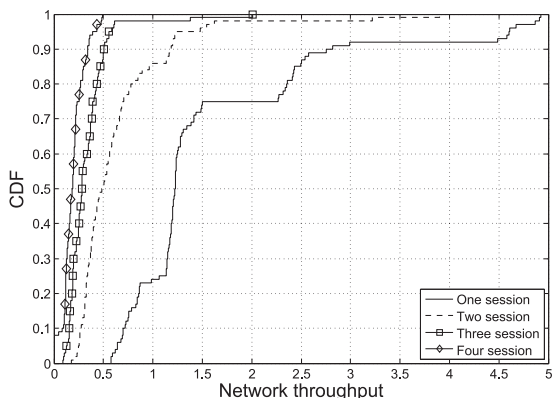


(a) The number of sessions increases from 1 to 4.

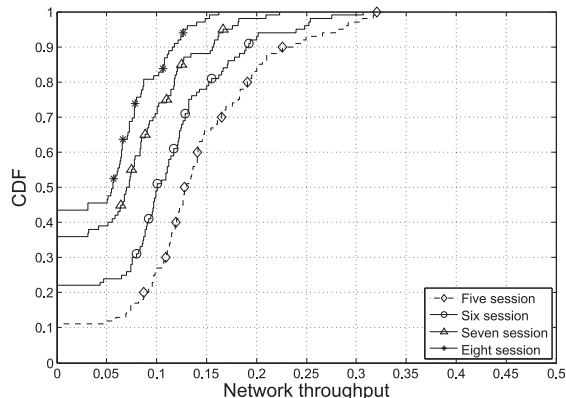


(b) The number of sessions increases from 5 to 8.

Fig. 6. CDF of achievable throughput under FD when the number of sessions varies from 1 to 8. Each curve is based on 100 randomly generated network instances, each with 30-nodes.



(a) The number of sessions increases from 1 to 4.



(b) The number of sessions increases from 5 to 8.

Fig. 7. CDF of achievable throughput under HD when the number of sessions varies from 1 to 8. Each curve is based on 100 randomly generated network instances, each with 30-nodes.

system parameters, such as target approximation error, number of time slots, path loss parameter, and network size.

Target approximation error. We study the ratio between achievable throughput of FD and HD under different target approximation error. Figs. 9a to 9c present the distribution of the ratio between achievable throughput of FD and HD. Each curve is based on 100 randomly generated 30-node network instances under different estimation error (ϵ). The number of sessions in the network is set to 4 and there are

TABLE 4
Distribution of the Throughput Ratio between FD and HD Based on 100 30-Node Network Instances as the Number of Sessions Increases from 1 to 8

Session Number	Number of Network Instances with Throughput Ratio $\geq \gamma$			
	$\gamma = 1$	$\gamma = 2$	$\gamma = 3$	$\gamma = 4$
1	100	0	0	0
2	100	8	1	0
3	100	27	2	1
4	100	44	12	8
5	100	52	14	11
6	100	60	24	22
7	100	66	39	37
8	100	71	48	44

four time slots in a time frame. As shown in the figures, when ϵ is 1, 5 and 10 percent, there are 41, 43, and 46 percent of instances achieve a ratio greater than 2, respectively.

Number of time slots. We study the ratio between achievable throughput of FD and HD when the number of time slots is increased to 6. Fig. 10 presents the distribution of

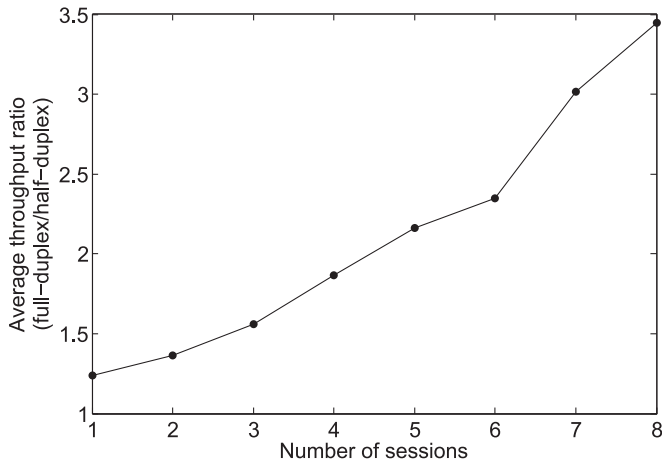


Fig. 8. Ratio between average achievable throughput of FD and HD when the number of sessions varies from 1 to 8. The average achievable throughput (for either FD or HD) is obtained over 100 network instances, each with 30 nodes. $T = 4$ time slots.

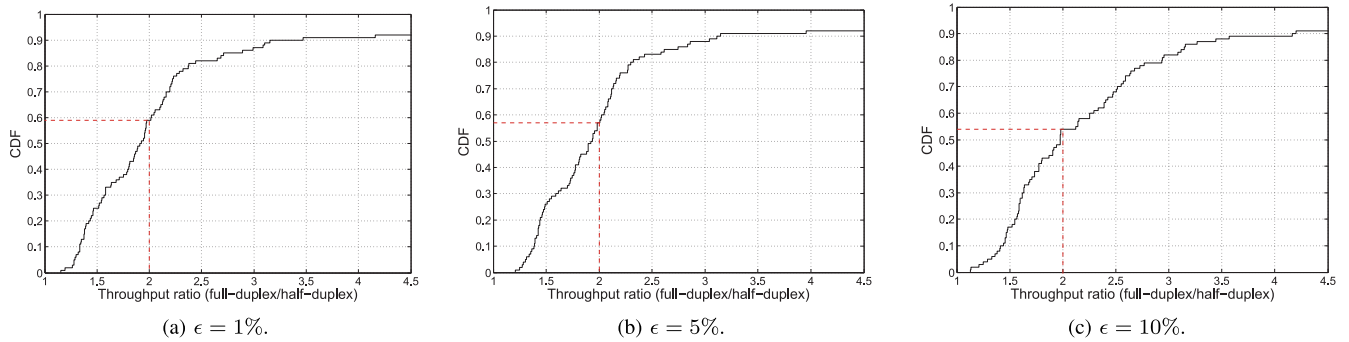


Fig. 9. CDF of the ratio between achievable throughput of FD and HD with different target approximation error. Each curve is based on 100 network instances, each with 30 nodes and four sessions. $T = 4$ time slots.

the ratio between achievable throughput of FD and HD based on 100 randomly generated 30-node network instances. The number of sessions in the network is set to 4. As shown in the figure, 17 percent of instances achieves a ratio greater than 2.

Network size. We study the the ratio between achievable throughput of FD and HD when the number of nodes in the network is increased to 50. Fig. 11 presents the distribution

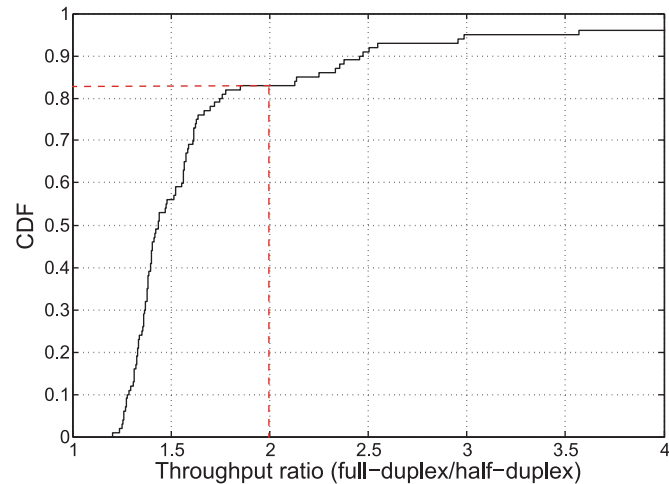


Fig. 10. CDF of the ratio between achievable throughput of FD and HD based on 100 network instances, each with 30 nodes and four sessions. $T = 6$ time slots.

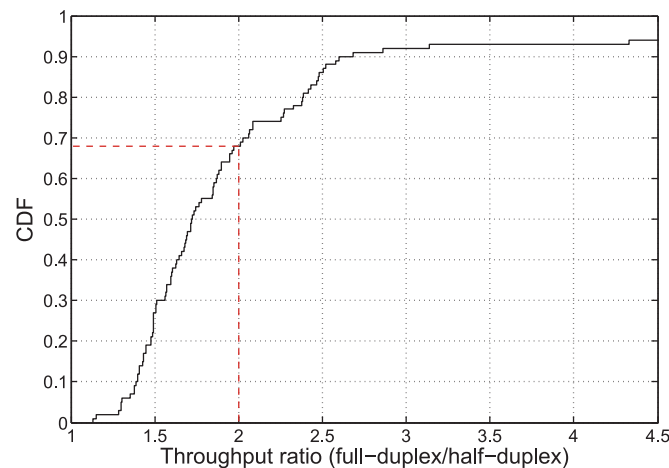


Fig. 11. CDF of the ratio between achievable throughput of FD and HD based on 100 network instances, each with 50 nodes and four sessions. $T = 4$ time slots.

of the ratio between achievable throughput of FD and HD based on 100 randomly generated 50-node network instances. The number of sessions in the network is set to 4 and there are 4 time slots in a time frame. As shown in the figure, 32 percent of instances achieves a ratio greater than 2.

Path loss parameter. We study the the ratio between achievable throughput of FD and HD when the path loss parameter is set to $g_{(Tx(k), Rx(l))} = [16.9 \log_{10}(d) + 40.4]$ (in dB) [42]. Fig. 12 presents distribution of the ratio between achievable throughput of FD and HD based on 100 randomly generated 30-node network instances. The number of sessions in the network is set to 4 and there are four time slots in a time frame. As shown in the figure, 39 percent of instances achieves a ratio greater than 2.

6 CONCLUSION

The benefits of FD for a single node in isolation were well understood. But the potential of FD on end-to-end throughput in a multi-hop wireless network was not well understood. This paper offered new results on this problem. Through rigorous mathematical modeling and formulation, we cast the end-to-end throughput problem under FD into an optimization problem. Using numerical results, we showed that session throughput in a FD network can exceed $2\times$ of that in a HD network in many cases. Our finding can be explained by the much larger scheduling space that is offered by removing HD constraints in the optimization problem. Our findings

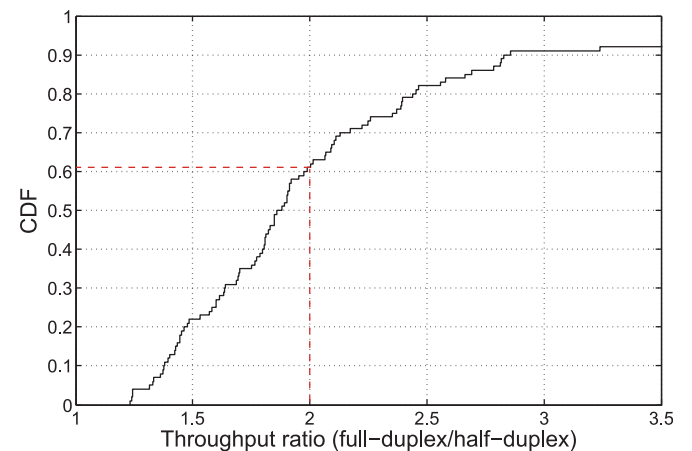


Fig. 12. CDF of the ratio between achievable throughput of FD and HD based on 100 network instances, each with 30 nodes and four sessions. $T = 4$ time slots. The path loss parameter is $[16.9 \log_{10}(d) + 40.4]$.

shed new light on the impact of node-level FD capability on network level end-to-end throughput performance.

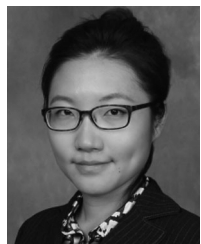
ACKNOWLEDGMENTS

This research was supported in part by NSF grants 1443889, 1343222, 1064953, and ONR grant N00014-15-1-2926. Part of Prof. W. Lou's work was completed while she was serving as a program director at the US National Science Foundation (NSF). Any opinion, findings, and conclusions or recommendations expressed in this paper are those of the authors and do not reflect the views of the NSF. The authors thank Virginia Tech's Advanced Research Computing for giving them access to the BlueRidge computer cluster. Y.T. Hou is the corresponding author.

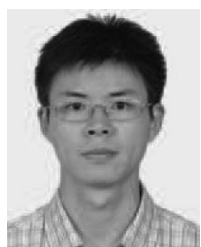
REFERENCES

- [1] D. Bharadia, E. McMillin, and S. Katti, "Full duplex radios," in *Proc. ACM Conf. Appl., Technol., Archit., Protocols Comput. Commun.*, Aug. 2013, pp. 375–386.
- [2] J. I. Choi, M. Jain, K. Srinivasan, P. Levis, and S. Katti, "Achieving single channel, full duplex wireless communication," in *Proc. ACM Annu. Int. Conf. Mobile Comput. Netw.*, Sept. 2010, pp. 1–12.
- [3] D. Bharadia and S. Katti, "Full duplex MIMO radios," in *Proc. USENIX Conf. Netw. Syst. Design Implementation*, Apr. 2014, pp. 359–372.
- [4] M. Jain, J. I. Choi, T. Kim, D. Bharadia, S. Seth, K. Srinivasan, P. Levis, S. Katti, and P. Sinha, "Practical, real-time, full duplex wireless," in *Proc. ACM Annu. Int. Conf. Mobile Comput. Netw.*, New York, NY, USA, Aug. 2011, pp. 301–312.
- [5] J. Kim, O. Mashayekhi, H. Qu, M. Kazandjieva, and P. Levis. (2013). Janus: A novel mac protocol for full duplex radio. Stanford Univ., Stanford, CA, USA. Tech. Rep., [Online]. Available: <http://web.stanford.edu/skatti/pubs/mobicom10-fd.pdf>
- [6] A. Sahai, G. Patel, and A. Sabharwal. (2011). Pushing the limits of full duplex: Design and real-time implementation. Rice Univ., Houston, TX, USA, Tech. Rep. [Online]. Available at <http://arxiv.org/abs/1107.1276>
- [7] M. Fukumoto and M. Bandai, "MIMO full-duplex wireless: Node architecture and medium access control protocol," in *Proc. 7th Int. Conf. Mobile Comput. Ubiquitous Network.*, Jan. 2014, pp. 76–77.
- [8] S. Goyal, P. Liu, O. Gurbuz, E. Erkip, and S. Panwar, "A distributed MAC protocol for full duplex radio," in *Proc. Asilomar Conf. Signals, Syst. Comput.*, Pacific Grove, CA, USA, Nov. 2013, pp. 788–792.
- [9] W. Cheng, X. Zhang, and H. Zhang, "RTS/CTS mechanism based full-duplex MAC protocol for wireless networks," in *Proc. IEEE GLOBECOM*, Atlanta, GA, USA, Dec. 2013, pp. 5017–5022.
- [10] S. Kim and W. E. Stark, "On the performance of full duplex wireless networks," in *Proc. 47th Annu. Conf. Inf. Sci. Syst.*, Baltimore, MD, USA, Mar. 2013, pp. 1–6.
- [11] X. Xie and X. Zhang, "Semi-synchronous channel access for full-duplex wireless networks," in *Proc. IEEE Int. Conf. Netw. Protocols*, Raleigh, NC, USA, Oct. 2014, pp. 209–214.
- [12] W. Zhou, K. Srinivasan, and P. Sinha, "RCTC: Rapid concurrent transmission coordination in full duplex wireless networks," in *Proc. IEEE Int. Conf. Netw. Protocols*, Goettingen, Germany, Oct. 2013, pp. 1–10.
- [13] K. Tamaki, H. Ari Raptino, Y. Sugiyama, M. Bandai, S. Saruwatari, and T. Watanabe, "Full duplex media access control for wireless multi-hop networks," in *Proc. IEEE 77th Veh. Technol. Conf.*, Dresden, Germany, Jun. 2013, pp. 1–5.
- [14] Z. Tong and M. Haenggi, "Throughput analysis for full-duplex wireless networks with imperfect self-interference cancellation," *IEEE Trans. Commun.*, vol. 63, no. 11, pp. 4490–4500, Aug. 2015.
- [15] J. Lee and T. Q. S. Quek, "Hybrid full-/half-duplex system analysis in heterogeneous wireless networks," *IEEE Trans. Wireless Commun.*, vol. 13, no. 5, pp. 2883–2895, May 2015.
- [16] S. Wang, V. Venkateswaran, and X. Zhang, "Exploring full-duplex gains in multi-cell wireless networks: A spatial stochastic framework," in *Proc. IEEE INFOCOM*, Hong Kong, China, May 2015, pp. 855–863.
- [17] T. K. Baranwal, D. S. Michalopoulos, and R. Schober, "Outage analysis of multihop full duplex relaying," *IEEE Commun. Lett.*, vol. 17, no. 1, pp. 63–66, Jan. 2013.
- [18] X. Fang, D. Yang, and G. Xue, "Distributed algorithms for multipath routing in full-duplex wireless networks," in *Proc. 8th IEEE Int. Conf. Mobile Ad-Hoc and Sensor Syst.*, Valencia, Spain, Oct. 2011, pp. 102–111.
- [19] B. Mahboobi and M. Ardebilipour, "Joint power allocation and routing in full-duplex relay network: An outage probability approach," *IEEE Commun. Lett.*, vol. 17, no. 8, pp. 1497–1500, Aug. 2013.
- [20] D. Ramirez and B. Aazhang, "Optimal routing and power allocation for wireless networks with imperfect full-duplex nodes," *IEEE Trans. Wireless Commun.*, vol. 12, no. 9, pp. 1536–1276, Sep. 2013.
- [21] Y. Yang and N. B. Shroff, "Scheduling in wireless networks with full-duplex cut-through transmission," in *Proc. IEEE INFOCOM*, Hong Kong, China, May 2015, pp. 2164–2172.
- [22] X. Xie and X. Zhang, "Does full duplex double the capacity of wireless networks," in *Proc. IEEE INFOCOM*, Toronto, Canada, Apr. 2014, pp. 253–261.
- [23] D. Kim, H. Lee, and D. Hong, "A survey of in-band full-duplex transmission: From the perspective of PHY and MAC layers," *IEEE Commun. Surveys Tuts.*, vol. 17, no. 4, pp. 2017–2046, Feb. 2015.
- [24] M. Duarte and A. Sabharwal, "Full-duplex wireless communications using off-the-shelf radios: Feasibility and first results," in *Proc. Asilomar Conf. Signals, Syst. Comput.*, Pacific Grove, CA, USA, Nov. 2010, pp. 1558–1562.
- [25] S. Hong, J. Mehlman, and S. Katti, "Picasso: Flexible RF and spectrum slicing," in *Proc. ACM SIGCOMM*, New York, NY, USA, Aug. 2012, pp. 37–48.
- [26] E. Aryafar, M. A. Khojastepour, K. Sundaresan, S. Rangarajan, and M. Chiang, "MIDU: Enabling MIMO full duplex," in *Proc. ACM Annu. Int. Conf. Mobile Comput. Netw.*, Istanbul, Turkey, Aug. 2012, pp. 257–268.
- [27] E. Everett, M. Duarte, C. Dick, and A. Sabharwal, "Empowering full-duplex wireless communication by exploiting directional diversity," in *Proc. Asilomar Conf. Signals, Syst. Comput.*, Pacific Grove, CA, USA, Nov. 2011, pp. 2002–2006.
- [28] E. Everett, A. Sahai, and A. Sabharwal, "Passive self-interference suppression for full-duplex infrastructure nodes," *IEEE Trans. Wireless Commun.*, vol. 13, no. 2, pp. 680–694, Oct. 2013.
- [29] M. A. Khojastepour, K. Sundaresan, S. Rangarajan, X. Zhang, and S. Barghi, "The case for antenna cancellation for scalable full-duplex wireless communications," in *Proc. 10th ACM Workshop Hot Topics Netw.*, New York, NY, USA, 2011, pp. 1–6.
- [30] M. Duarte, C. Dick, and A. Sabharwal, "Experiment-driven characterization of full-duplex wireless systems," *IEEE Trans. Wireless Commun.*, vol. 11, no. 12, pp. 4296–4307, Dec. 2012.
- [31] M. Duarte, A. Sabharwal, V. Aggarwal, R. Jana, K. K. Ramakrishnan, C. W. Rice, and N. K. Shankaranarayanan, "Design and characterization of a full-duplex multi-antenna system for WiFi networks," *IEEE Trans. Veh. Technol.*, vol. 63, no. 3, pp. 1160–1177, Mar. 2014.
- [32] B. Radunovic, D. Gunawardena, P. Key, A. Proutiere, N. Singh, V. Balan, and G. Dejean, "Rethinking indoor wireless mesh design: Low power, low frequency, full-duplex," in *Proc. IEEE 5th IEEE Workshop Wireless Mesh Netw.*, Boston, MA, USA, Jun. 2010, pp. 1–6.
- [33] E. Ahmed, A. Eltawil, and A. Sabharwal, "Self-interference cancellation with nonlinear distortion suppression for full-duplex systems," in *Proc. Asilomar Conf. Signals, Syst. Comput.*, Pacific Grove, CA, USA, Nov. 2013, pp. 1199–1203.
- [34] M. A. Khojastepour and S. Rangarajan, "Wideband digital cancellation for full-duplex communications," in *Proc. Asilomar Conf. Signals, Syst. Comput.*, Pacific Grove, CA, USA, Nov. 2012, pp. 1300–1304.
- [35] T. Riihonen, S. Werner, and R. Wichman, "Residual self-interference in full-duplex MIMO relays after null-space projection and cancellation," in *Proc. Asilomar Conf. Signals, Syst. Comput.*, Pacific Grove, CA, USA, Nov. 2010, pp. 653–657.
- [36] C. Perkins, E. Belding-Royer, and S. Das, "Ad hoc on-demand distance vector (AODV) routing," IETF RFC 3561, Jul. 2003.
- [37] D. B. Johnson, D. A. Maltz, and J. Broch, "DSR: The dynamic source routing protocol for multi-hop wireless ad hoc networks," in *Ad Hoc Networking*. Boston, MA, USA: Addison-Wesley, 2001.

- [38] Y. T. Hou, Y. Shi, and H. D. Sherali, *Applied Optimization Methods for Wireless Networks*. Cambridge, U.K.: Cambridge Univ. Press, 2014.
- [39] G. L. Nemhauser and L. A. Wolsey, *Integer and Combinatorial Optimization*. New York, NY, USA: Wiley, 1999.
- [40] IBM ILOG CPLEX: A commercial software [Online]. Available: <http://www.ibm.com/software/integration/optimization/cplex/>
- [41] ETSI TR 125 942 (V3.3.0): Universal Mobile Telecommunications System (UMTS); RF system scenarios (3GPP TR 25.942 version 3.3.0).
- [42] ITU-R TR M.2135-1: Guidelines for evaluation of radio interface technologies for IMT-Advanced.



Xiaoqi Qin received the BS and MS degrees in computer engineering from Virginia Tech, Blacksburg, VA, USA, in 2011 and 2013, respectively. Since Fall 2013, she has been working toward the PhD degree in the Bradley Department of Electrical and Computer Engineering, Virginia Tech. Her current research interest include algorithm design and cross-layer optimization for wireless networks. She is a student member of the IEEE.



Huacheng Zeng received the BE and MS degrees in electrical engineering from the Beijing University of Posts and Telecommunications (BUPT), Beijing, China, in 2007 and 2010, respectively. He received the PhD degree in computer engineering from Virginia Tech, Blacksburg, VA, USA, in 2015. He is currently a senior system engineer at Marvell Semiconductor, Santa Clara, CA, USA. His research interests include high-throughput, energy-efficient, and attack-resilient protocol design for wireless networks. He received the ACM WUWNET 2014 Best Student Paper Award. He is a member of the IEEE.



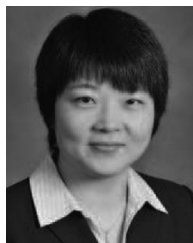
Xu Yuan received the BS degree in computer science from Nankai University, Tianjin, China, in 2009. Since Fall 2010, he has been working toward the PhD degree in the Bradley Department of Electrical and Computer Engineering, Virginia Tech, Blacksburg, VA, USA. His current research interests include algorithm design and optimization for cognitive radio networks. He is a member of the IEEE.



Brian Jalaeian received the MS degrees in electrical engineering and industrial system engineering (operation research) from Virginia Tech, Blacksburg, VA, USA, in 2013 and 2014, respectively. He is currently working toward the PhD degree in the Bradley Department of Electrical and Computer Engineering, Virginia Tech. His research interests include the application of optimization and operation research in complex wireless communication system and network problems. He is a member of the IEEE.



Y. Thomas Hou (F'14) received the PhD degree from NYU Polytechnic School of Engineering (formerly Polytechnic Univ.), Brooklyn, NY, USA. He is the Bradley Distinguished Professor of Electrical and Computer Engineering at Virginia Tech, Blacksburg, VA, USA. His current research interests include developing innovative solutions to complex cross-layer optimization problems in wireless and mobile networks. He has published two graduate textbooks: *Applied Optimization Methods for Wireless Networks* (Cambridge, U.K.: Cambridge University Press, 2014) and *Cognitive Radio Communications and Networks: Principles and Practices* (San Francisco, CA, USA: Academic, 2009). He is the Steering Committee Chair of IEEE INFOCOM conference and a member of the IEEE Communications Society Board of Governors. He is a fellow of the IEEE.



Wenjing Lou (F'15) received the PhD degree in electrical and computer engineering from the University of Florida, Gainesville, FL, USA. She is a professor in the Computer Science Department at Virginia Tech. Her research interests include the broad area of wireless networks, with special emphases on wireless security and cross-layer network optimization. Since August 2014, she has been serving as a program director at the US National Science Foundation. She is the Steering Committee Chair of the IEEE Conference on Communications and Network Security (CNS). She is a fellow of the IEEE.



Scott F. Midkiff is a professor & vice president for information technology and chief information officer at Virginia Tech, Blacksburg, VA, USA. From 2009 to 2012, he was the department head of the Bradley Department of Electrical and Computer Engineering, Virginia Tech. From 2006 to 2009, he served as a program director at the US National Science Foundation. His research interests include wireless and ad hoc networks, network services for pervasive computing, and cyber-physical systems. He is a senior member of the IEEE.

▷ For more information on this or any other computing topic, please visit our Digital Library at www.computer.org/publications/dlib.